International Journal of Modern Physics A
Vol. 36, Nos. 11 & 12 (2021) 2140013 (16 pages)

DOI: 10.1142/S0217751X21400133

First result of orbit verification of Taiji-1 hall micro thruster

Shu-Yan Xu[*,†], Lu-Xiang Xu[*,‡], Lin-Xiao Cong[‡], Yong-Gui Li[‡] and Cong-Feng Qiao[‡,§]

[*]*Center for Space Propulsion and Gravitational Universe (SPaGU), School of Fundamental Physics and Mathematical Sciences, Hangzhou Institute for Advanced Study, UCAS, Hangzhou 310024, China*

[†]*Plasma Sources and Application Centre and Space Propulsion Center, NIE, Nanyang Technological University, 1 Nanyang Walk, 637616, Singapore*

[‡]*Taiji Laboratory for Gravitational Wave Universe (Beijing/Hangzhou), University of Chinese Academy of Sciences (UCAS), Beijing 100049, China*
[§]*qiaocf@ucas.ac.cn*

[¶]*On behalf of The Taiji Scientific Collaboration*

Received 15 September 2020
Accepted 30 October 2020
Published 29 March 2021

The Hall Micro Thrusters (HMTs) use cold gas or accelerated plasma dual mode to provide ultra-precise spacecraft altitude control. They were operated in space for the first time as part of the demonstration payloads on Chinese Academy of Science's (CASs) Taiji-1 spacecraft since September 2019. Hall Micro Thruster Assemblies (HMTAs) were the actuators in drag-free control, and will compensate the nonconservative force for gravity wave observatories. The HMTAs meet the requirements of operating at 5–100 μN of thrust with 0.7 μN resolution and $\leq$0.6 μN/Hz$^{1/2}$ (0.01–1 Hz) noise to deliver the nanometer-level precision control as fast as 30 ms measured by Gravitational Reference Sensor (GRS). A transfer function model in z-domain was fit and used to filter HMTs cathode voltage to predict GRSs thrust noise response. Simulations of a single or dual-frequency disturbance and the corresponding compensation demonstrated that HMTAs could deliver the required thrust profile expected. The capability to meet the requirements of thruster noise in drag-free control is critical for future missions because the acceleration noise on test mass directly relates to the gravity wave signa l**.** Preliminary in-orbit verification of Taiji-1 has showed HMTAs' great potential in future, and the data in the experiments are presented in this paper.

1. Introduction

Gravitational waves are ripples in the fabric of space–time, which were first proposed by Albert Einstein and were directly detected for the first time by the Laser Interferometer Gravitational Wave Observatory (LIGO)[1] on September 14, 2015. To detect the gravitational waves in the frequency range 0.1 mHz–1 Hz, which are beyond the LIGO

[§]Corresponding author.
[¶]For more details, please refer to article 2102002 of this Special Issue.

detection capability, European Space Agency proposed a space-borne gravitational wave program, the Laser Interferometry Space Antenna (LISA).[2] To this aim as well, in a bit later time China also put forward a program, the Taiji Project,[3–6] which is expected to have higher detection sensitivity than LISA in the 0.01–1 Hz band. The Taiji-1 satellite, a pathfinder for key technology verification, was launched on August 31, 2019,[7] which is China's first gravitational wave detection key technology verification satellite. Its core payloads include laser interferometer,[8] drag-free control module,[9] three-axis electrostatically suspended accelerometer or gravitational reference sensor (GRS),[10] radio frequency ion micro thruster (RIT)[11,12] and Hall Micro Thrusters (HMT),[13–15] and has completed a series of space science experiments of great values.

In order to detect the weak gravitational waves, it is necessary to offset the disturbance of nonconservative forces such as solar light pressure and atmospheric damping, so that the test mass of the satellite is in free fall, and micro thrusters are employed to achieve drag-free control. Taiji-1 uses RIT and HMT as engines, both mounted symmetrically on opposite sides of the satellite in a crossing configuration, enabling single, double or four thrusters firing in collaborative control process. The University of Chinese Academy of Sciences (UCAS), in cooperation with Nanyang Technology University (NTU), developed a first international dual-mode HMT, which can be either set as a cold gas micro thruster based on mass flow control or as an electrical micro thruster through the electric field acceleration of Xenon ions to obtain a higher particle injection speed, the process of which actually transforms solar energy into additional kinetic energy, issuing a higher specific impulse than conventional chemical thrusters. The magnetic field instead of the screen grid constrains the electrons, which greatly reduces the erosion of the channel and prolong the orbital life expectancy.

2. Principles

The HMTAs includes four thruster heads (A1, A2, B1 and B2), four high voltage supplies, two mass flow controllers and one Power Processing Unit (PPU). The thruster head consists of an internal fixed permanent magnet, a discharge chamber, an anode and the electron emitting surface made of special material, resulting in a simple design and structure lightweight. The mass flow control unit includes high pressure regulators, insulation valves, micro valves, pipes, standoffs & brackets and a low-pressure transducer. After the pressure regulation stage to provide a "low pressure" (nominal 0.2 Mpa) at the HMTAs inlet, the mass flow is controlled as low as 0.1 sccm during the thrust actuation stage, guaranteed 0.01 K temperature fluctuation accuracy. The PPU supplies power to high voltage supplies and mass flow controllers, communicates with the microcontroller unit and the host computer by sending and receiving signals such as thrust instruction, operating mode, feedback voltage, current, pressure, etc.

HMT combines cold electron emission and Hall effect, using a highly integrated design with complementary and integrated features, such as high stability, ultra-precision, fast response, light weight, compact volume, moderate specific impulse and low risk of plasma plume pollution. Field emission electrons ionize xenon gas to form a low-density

plasma, and the electrons are constrained by the magnetic field forming a cathode at the outlet. By means of the kinetic energy generated by the interaction between radial magnetic field and axial electric field, the angular moving electrons and atoms collide to exchange energy further, and the Xenon gas almost realizes complete ionization. Before ions escaping from the quasi-neutral ring, they are accelerated by the electric field and neutralized by electrons as they ejected into space at high speed, which forms a reaction force that pushes the spacecraft.

To ensure drag-free control, the HMT thrust ranges from 5 μN to 50 μN, with resolution less than 1.5 μN, noise lower than 1.5 μN/Hz$^{1/2}$ within the low-frequency band (0.01–1 Hz), and the response time is less than 50 ms. Based on electrostatic ions' acceleration, HMT optimizes the magnetic field to constrain Xenon plasma to reduce wall erosion. After the gas supply is stabilized, the mass flow is controlled by the micro regulator valve, and high voltage is proportionally output to ionize and accelerate the Xenon to achieve high specific impulse, greatly reducing the propellant consumption. In the worst situation of high voltage power failure, HMT can still degenerate into a cold gas thruster, providing a backup for drag-free control.

3. Test Overview

Since entering the orbit, HMTAs have worked for hundreds of hours, and have successively completed hundreds of experiments, such as gas leak testing, high voltage load testing, single, double and fully ignition, in-orbit calibration for mass flow and voltage using lookup table for thrust, thrust range, thrust resolution, thrust noise and response time test in cold gas or electric propulsion mode. In addition, HMTAs' thrust disturbance and compensation experiments with single/dual frequency were verified to demonstrate drag-free operations. In detail, the temperatures of GRS and HMTAs are controlled during the experiment process. The Taiji-1 satellite stops attitude control such as cold gas, magnetic control and momentum wheel, after the transition from earth oriented into "free drift" mode. The thrust command sequence is sent by the satellite CPU and GRS records the acceleration results of motion caused by micro propulsion and other nonconservative forces.

3.1. *Thrust measurement*

Thrust measurements are made via both direct and indirect methods. Direct method measures acceleration resulting from the thrust on the satellite, while indirect thrust measurements analyzes the relationship between thrust and voltage-current-mass flow. The in-orbit test of HMTAs relies on the feedback acceleration from the inertial sensor, whose capacitance between electrode and test mass is modulated by external forces. The equivalent acceleration is calculated by the difference of capacitance voltage for different distances that can be obtained by multiplying the satellite mass.[16] Meanwhile, the HMTAs can monitor its own load current, cathode voltage, air pressure, temperature states under different valve's open time and high voltage configuration, and establish a

map between electrical parameters and thrust value with mass flow binary tree, providing an alternative to observe the thrust. In addition, the thrust can be also measured by Xenon free molecules flow through the orifice in cross-validation with the GRS measurement results.[17]

3.2. *Thrust accuracy calibration*

In order to eliminate the thrust inconsistencies between in-orbit and ground calibration, HMT needs to be calibrated with inertial reference sensor before formal test. To identify the impacts of variables such as orbit environment, instrument temperature and other factors, the Taiji-1 satellite chooses to drift near the magnetic equator to avoid residual magnetic disturbances, measures the thrust repeatedly in multiple orbits, and uses low-pass filter or moving mean method to improve the accuracy. By setting "0" thrust mark while tracing the zero drift between the measured adjacent thrust values, the test data is detrended according to the calibrated increment. Thrust sequence with incremental step containing "0" reference is injected to HMT, after which the combination of high-voltage input and mass flow is recorded. States such as temperature, pressure and cathode voltage relevant to thrust are collected by PPU updating the lookup table to keep the thrust input consistent with GRS output. According to the 50 μN calibration results of GRS, the residual error between the steady-state measurements and the thrust instructions is less than 1 μN, considering the background noise ranged from 0.01 Hz to 1 Hz. Meanwhile, the thrust resolution of HMTAs own electric telemetry parameters will increase in the region where thrust values have a good relationship to the function of the mass flow and voltage. By interpolating the configuration parameters such as high voltage input, switch cycle and valve's open time duty ratio, expected output thrust precision of the lookup table reaches 0.1 μN, which meets the demand of Taiji-1 satellite mission.

4. Thruster Performance

4.1. *Thrust range*

HMT can work in cold gas propulsion mode or electric acceleration mode. The thrust range of the cold gas propulsion mode is 0.1–150 μN by tuning the mass flow, while the thrust range under the electric field acceleration covers 5–100 μN, which is constrained by the high voltage input and mass flow adaptation. As shown in Fig. 1, after the satellite was set to free-drift mode, the thrust of HMT-A2 was instructed to rise from 2 μN to 105 μN, which was detected by the 100 Hz acceleration data of X1, X2 and X3 channel of GRS. The experiment results showed that the thrust input was in accord with the weighted thrust, which was smoothed by 1.5 s, converted by mass and scale factor. Except for the huge impact of cold gas when the valve was initially opened, the thrust steps of HMT-A2 were clear and distinguishable based on the zero thrust regression point. As shown in Fig. 2, thrusters HMT-A1 and HMT-B1 in the opposite direction output 5, 10, 15, 20, 25, 30 μN one after another, where the thrust measurement in this process conforms to the instruction input.

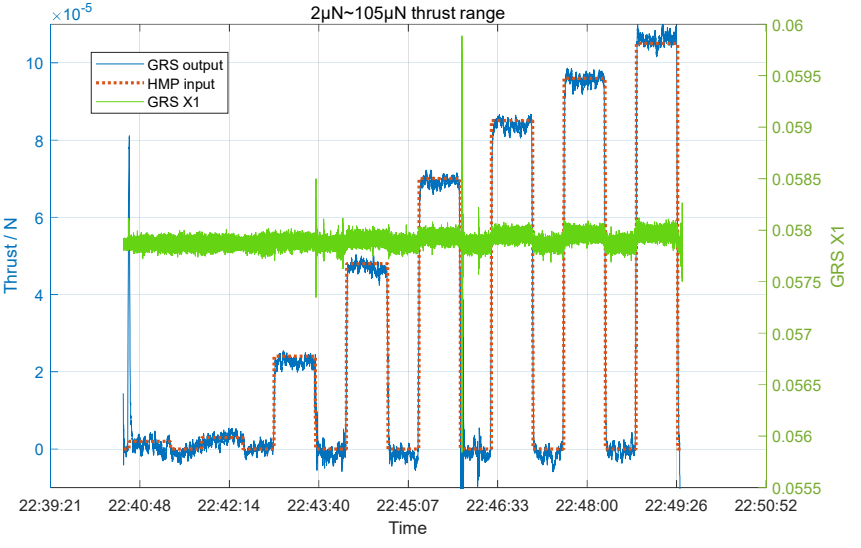

Fig. 1. HMT A2 outputs of 2–105 μN in cold gas mode.

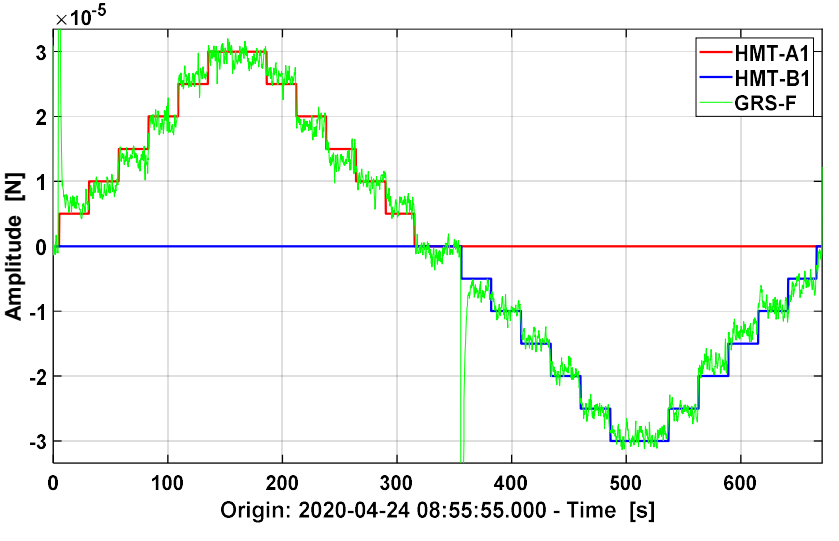

Fig. 2. Thrust step sequence of HMT-A1 and HMT-B1.

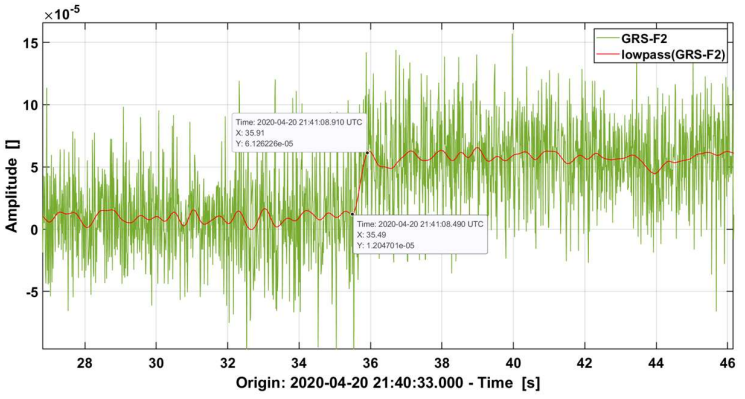

Fig. 3. 50 μN step measured by GRS after 1 Hz low pass filter (LPF).

4.2. *Thrust response time*

Thrust response time is an important indicator of the dynamic performance of micro-propulsion system. To measure the thrust response time of HMT, as shown in Fig. 3, thrusters HMT-A1 and HMT-A2 triggered the step response at the same time under the condition of constant flow, and the 1 Hz low-pass filtering of the GRS data feedback showed 50 μN increment, of which the thrust levels before and after the step were approximately 10 and 60 μN, respectively, so as to distinguish trend clearly. Due to the loss of high-frequency information on 1 Hz data, the 100 Hz data after 10 Hz low-pass filtering is repeated in Fig. 4, where there was a balance between trend recognition and high frequency changes. Taking 10% and 90% markers of response time as the criterion, according to the time stamps of 4.1 and 60 μN whose thrust step close to 50 μN, HMTs thrust response time in electric acceleration mode measured by GRS does not exceed 30 ms.

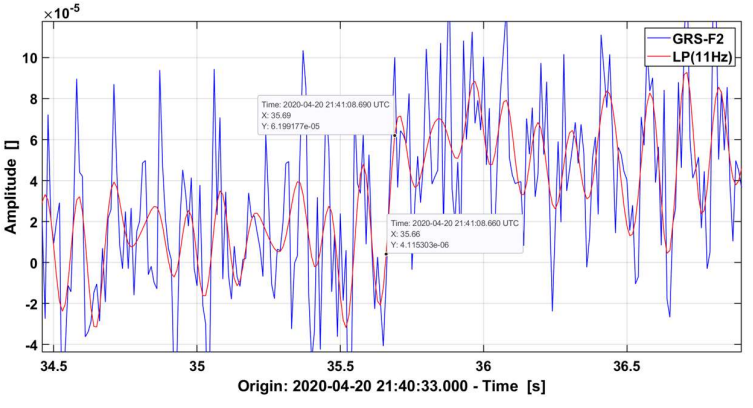

Fig. 4. 50 μN step measured by GRS after 10 Hz LPF.

4.3. *Thrust resolution*

The thrust resolution of HMT depends on how it is measured. Under electrostatic accelerometer measurement conditions, the thrust resolution of HMT in orbit is close to 0.5 μN. As shown in Fig. 5, when the thrust value switched between nominal 31 and 32 μN at 0.01 Hz in the form of square wave with duty ratio of 0.5, the load current switches between 0.186 and 0.164 A while the cathode feedback voltage between −0.177 and −0.2 V. These variables are both used to calculate the output thrust and still have a margin of quantitative accuracy of sampling, so the HMTs internal resolution accuracy of thrust configuration can be higher. On the other hand, matched filtering[18,19] with the square wave template was used in GRSs thrust resolution. Compared to the matched filtering, when square wave template was of amplitude 0.7 μN plus 3 μN random noise, the GRSs thrust data was found to fluctuate between 0.5–1 μN after being detrended to fit the drift and smoothed to weaken the high frequency oscillation. Considering the differences in the noise, the average level of thrust resolution evaluated in Fig. 6 is approximately 0.7 μN, consistent with the matching filter results when the Gaussian white noise input is added. Therefore, the thrust resolution of HMT is less than 0.5 μN, both in terms of the internal feedback and the external GRS.

4.4. *Thrust noise and decoupling*

HMTs thrust noise is measured directly using inertial sensors and evaluated by internal state telemetry. When using the inertial sensors, the thrust noise is measured on a chain

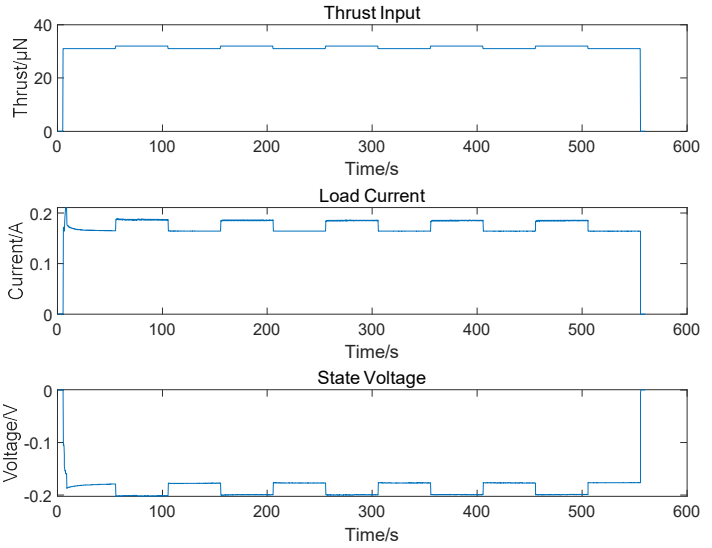

Fig. 5. Load current and state voltage varied as thrust input switched between 31 and 32 μN.

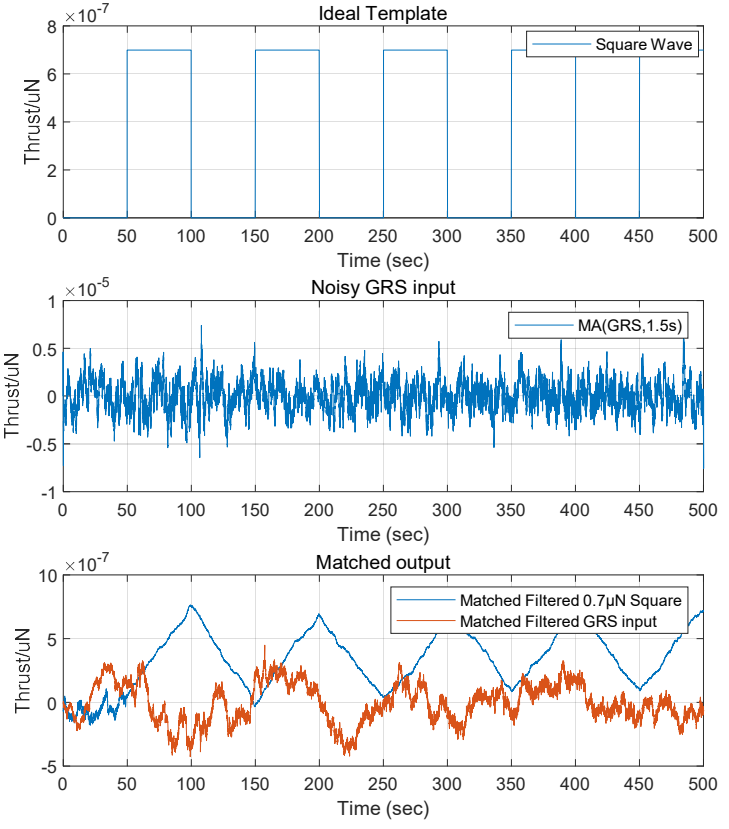

Fig. 6 Thrust resolution of 0.7 μN based on matched filtering.

starting from the thruster output, through the atmospheric damping, solar radiation, residual magnetism moment and other external force disturbance, to the inertial sensors where all disturbances finally coupled as the relative motion of the test mass under electrostatic modulation. Whereas, the mass flow, voltage and current of HMT can also be used to calculate the thrust and are not affected by the chain's coupling factors. Thus, this study focuses on state telemetry to evaluate the peak thrust noise.

The thrust noise of HMT is required to be small in order to keep the spacecraft in motion. For a thrust of 10 μN in electric acceleration mode for 300 s, 100 Hz GRS data weighted average on X1, X2 and X3 channels was filtered by a 2 Hz LPF and down sampled to 4 Hz. Force ASD using Kaiser window[20] reached its maximum 2.7 μN/Hz$^{1/2}$ at 0.019 Hz as shown in Fig. 7, which was higher than test on ground because of the unconservative force disturbances coupled during the measurement chain. Luckily,

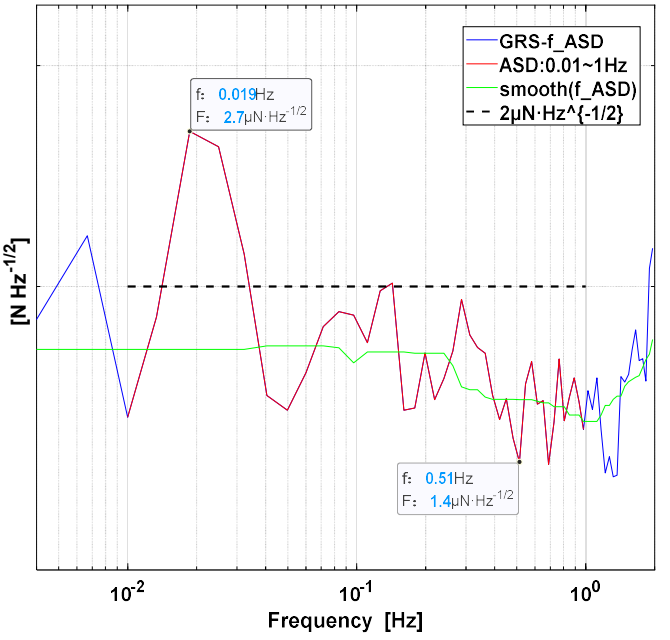

Fig. 7. Thrust ASD in the frequency range of 0.01–1 Hz.

by observing intrinsic vibration peaks of HMTs internal feedback states such as load current and cathode voltage, the transfer function to thrust could be used to filter their contribution.

For example, when the valve's switch cycle was configured as 0.2868 s, a beat formed between equivalent switch frequency and driving frequency 4 Hz. Based on the cathode voltage of HMT-A1 and GRSs force measured during 200–500 s, see in Fig. 8, the ASD of cathode related voltage and 100 Hz GRSs force after a 2 Hz LPF (down sampled to 4 Hz) were, respectively, shown in Fig. 9, where the beat frequency can be calculated as follows:

$$f_b = \frac{10^6}{286800} - 4 \approx 0.51 \text{ Hz}.$$

As shown in the upper diagram of Fig. 9, there were two peaks on the ASD of cathode related voltage. The one near 0.02 Hz was drift of cathode voltage, and the other one at 0.51 Hz was the beat formed by valve's switch and electromagnetic force. Whereas, the lower diagram of Fig. 9 showed that the force ASD at 0.51 Hz was 1.4 μN/Hz$^{1/2}$, which did not peak as well as HMTs internal thrust indicator, for its readout coupled with other unknown external forces. The other peak at 0.019 Hz was 2.6 μN/Hz$^{1/2}$ and somehow consistent with HMTs internal thrust indicator. But to

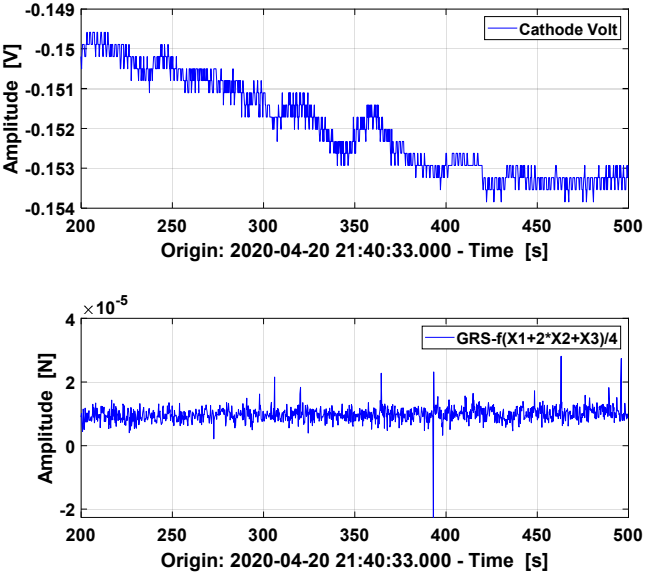

Fig. 8. Cathode voltage and thrust measured by GRS during 200–500 s.

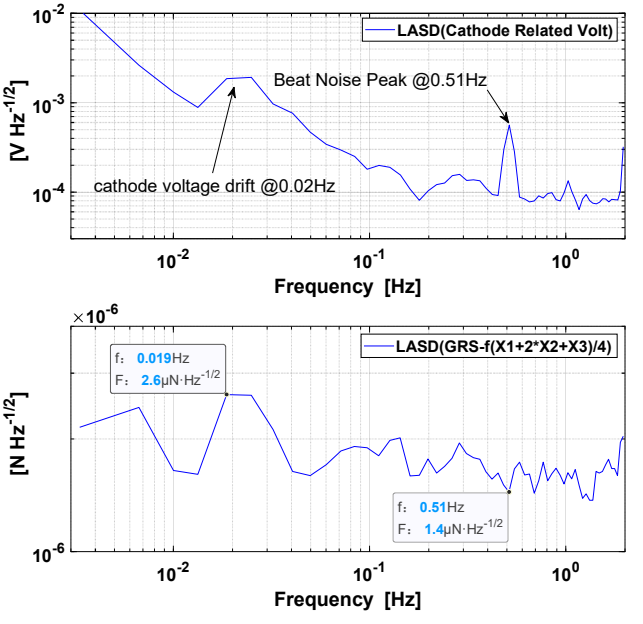

Fig. 9. Cathode voltage and GRS ASD in the frequency range 0.01–1 Hz.

precisely tell the difference between HMTs net thrust and GRS resultant force, transfer function estimation based on cathode voltage and force data is critical for assessing the contribution.

To estimate the real thrust level of HMT, system identification in z-domain was performed to fit transfer function model's desired parameters and reconstruct thrust after digital filtering. In detail, 100 Hz GRS force data was smoothed in a span of 100 ms, filtered by a 4 Hz LPF, and down sampled to 4 Hz to match the sampling frequency of the cathode voltage, which was detrended before estimating the transfer function. For the meaningful frequency region in the range 0.001–4 Hz, the transfer function was split to extract only meaningful data to start the fitting process, after which the cathode voltage data was filtered with the fit output in order to extract HMTs net thrust. As shown in Fig. 10, thrust ASD transferred from HMTs cathode voltage was only 0.28 μN/Hz$^{1/2}$ at 0.51 Hz and only 0.6 μN/Hz$^{1/2}$ at 0.019 Hz, well below the level at the same frequency measured by GRS. And the same is true to HMTs load current, pressure, etc. Therefore, the real thrust noise of HMT meets the requirements of drag free, on condition that the residual noise of GRS could be decoupled.

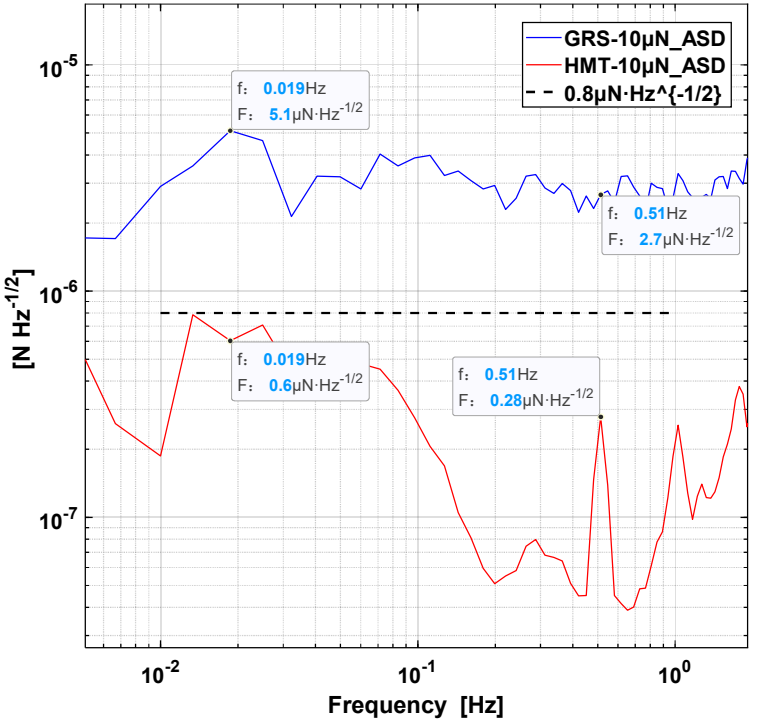

Fig. 10. Comparison of GRS ASD with or without cathode voltage contribution.

5. Thrust Disturbance and Compensation

According to the real-time feedback of the control loop, the thrust compensation is calculated to realize drag-free control. In order to verify the disturbance compensation of HMT, the in-orbit experiment was designed to modulate the HMT on one side to send out disturbance thrust signal, and to compensate the variation in the corresponding frequency band of HMT on the opposite side. Here, the experiments included unilateral single-frequency disturbance, bilateral single-frequency disturbance — compensation, bilateral dual-frequency disturbance — single frequency compensation and so on. Sequential sinusoids were discretely quantified in terms of five or more orders of thrust, with each frame sent out at unequal time interval and appropriate phase delay. GRS thrust series and its frequency domain performance validated whether HMT was effective in drag-free control.

5.1. *Single-Frequency Disturbance*

Using the thrust instruction sequence, HMT can produce periodic disturbance signal on side of the satellite. As shown in Fig. 11, the thrust output of HMT-A2 was modulated as a sine wave in a period of 12 s, which oscillated between 10 and 30 μN, and calmed down to 20 μN after nine cycles. Relative to the beginning and end of the thrust sequence, the thrust measured by GRS after 0.01–0.25 Hz bandpass filtering was basically consistent with the input. The background fitted by a 2-order polynomial was subtracted, and Kaiser window was used to control the peak side lobe level (PSLL) lower. The peak frequency of thrust ASD measured by GRS was 0.0865 Hz corresponding to the spectrum in Fig. 12, which was very close to the frequency point of 0.0833 Hz, i.e. the inverse of a period of 12 s.

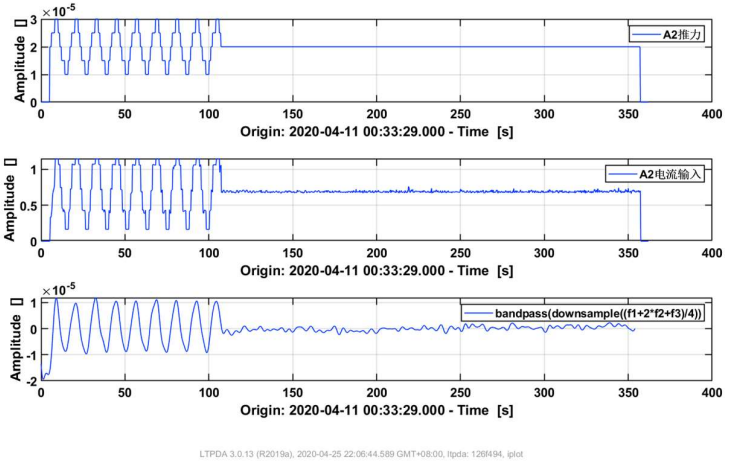

Fig. 11. HMT-A2 was modulated as a sine wave.

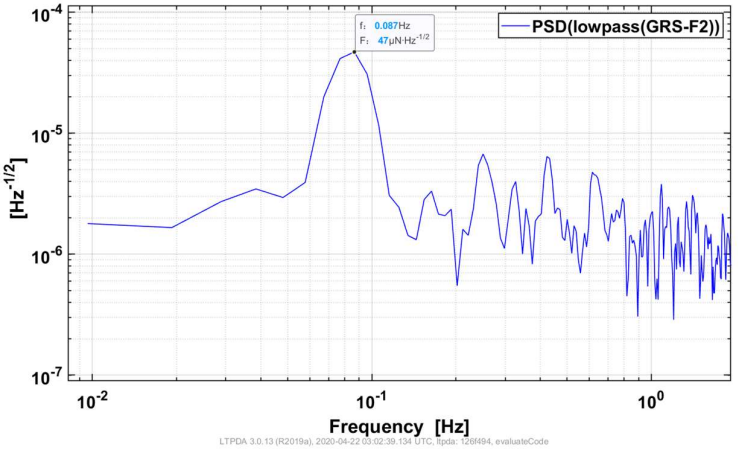

Fig. 12. Single-frequency disturbance of HMT-A2.

5.2. *Dual-frequency disturbance versus single-frequency compensation*

To validate the performance of HMTA in the drag-free control laws, in-orbit verification with a dual-frequency disturbance versus single-frequency compensation was conducted. As shown in Fig. 13, the thrust instruction sequence of HMT-A1, HMT-A2 and HMT-B1

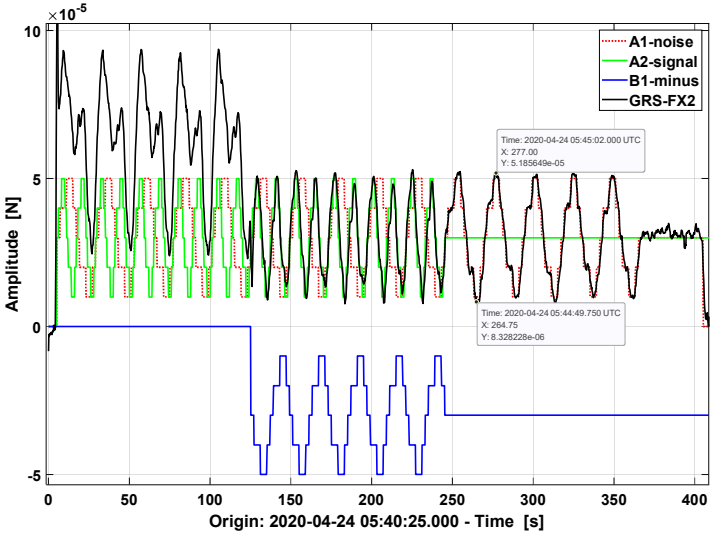

Fig. 13. Thrust instruction sequence of HMT-A1, A2 and B1.

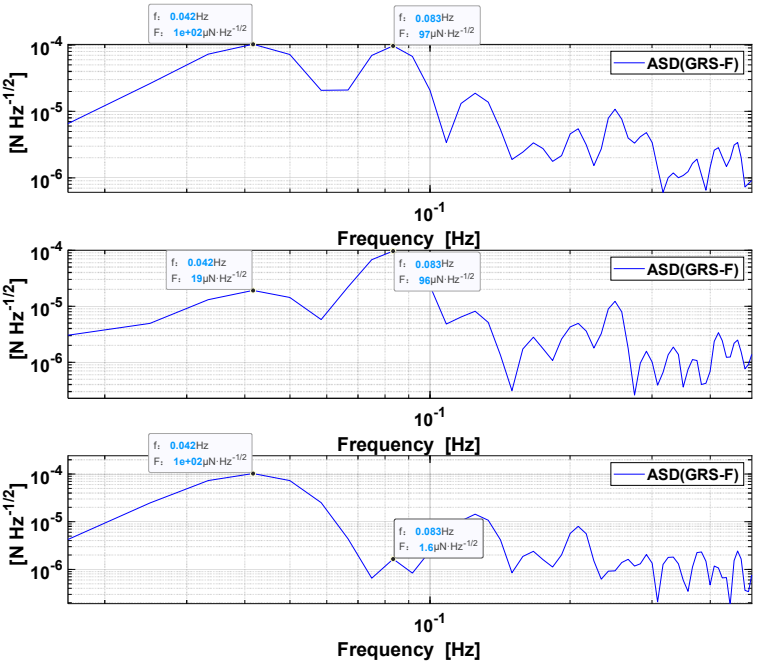

Fig. 14. Thrust ASD based on GRSs sensing of multiple thrusters.

was adjusted to produce a net force on the spacecraft in three stages, corresponding to three spectrums in Fig. 14 respectively measured by GRS after a bandpass filter of 0.01–0.25 Hz. During 6–124 s, the thrust of A1 and A2 was modulated at the same amplitude of 10–50 μN with the period of 24 and 12 s, meanwhile the GRS ASD after eliminated the low-frequency drift showed two peaks of close amplitude at 0.042 and 0.083 Hz, in accord with thrust instruction's modulation frequency of 0.0417 and 0.0833 Hz, indicating the output consistency of A1 and A2. With the occurrence of B1 thrust compensation and the cessation of A2 thrust, the noise amplitude of the two characteristic peaks fluctuated successively, and the amplitude of their separate occurrence was the same as that of their joint occurrence, indicating that B1 is accurate and effective for the disturbance compensation of A1 at the frequency of 0.042 Hz.

6. Conclusions

Preliminary orbit verification of Taiji-1 HMT demonstrated the HMTAs capability of drag-free control, including validation of the thruster technology using cold gas or electric acceleration dual modes, thrust performances and assessment algorithm based on GRS for the first time. The thrust range of HMTAs is 0.1–150 μN in cold gas mode by tuning the mass flow, or 5–100 μN in electric acceleration mode which is constrained by

high voltage input and mass flow combinations. HMTAs' thrust response time in electric acceleration mode measured by GRS for a 50 μN step is about 30 ms. The thrust resolution of 0.7 μN was also verified by direct measurement of GRS at the system level and through electric states monitoring at the individual thruster level. The thrust noise of HMTAs, though hardly to read out on original GRS data for unknown orbital disturbance, can be decoupled with HMT's internal states at the beat frequency by assessing the peak thrust contribution to GRS, and the residual ASD after z-domain fit is less than 0.6 μN/Hz$^{1/2}$ in frequency range of 0.01–0.1 Hz. To test HMTAs' performance in drag-free control, experiments were designed to modulate the HMT on one side to send out disturbance thrust signal in single/dual frequencies, and to compensate the variation in the corresponding frequency band of HMT on the opposite side, which showed a great success on the GRS ASD as the thrust pattern changed. In summary, HMT is one of the candidates for gravitational wave detection, and will provide even subtle thrust control by modeling the thrust noise. More details about this work will be discussed in the following papers, which will concentrate on the unique design in micro valves' control and cathodes' self-neutralization mechanism.

Acknowledgments

This work was supported in part by the Strategic Priority Research Program of the Chinese Academy of Sciences with Grant Nos. XDB23030100 and XDA15020700. Professor Xu and NTUs supports in HMTA are appreciated.

References

1. A. Abramovici, W. E. Althouse, R. W. P. Drever, Y. Gürsel, S. Kawamura, F. J. Raab, D. Shoemaker, L. Sievers, R. E. Spero, K. S. Thorne, R. E. Vogt, R. Weiss, S. E. Whitcomb and M. E. Zucker, *Science* **256**, 5055 (1992).
2. K. Danzmann and A. R diger, *Class. Quantum Grav.* **20**, S1–S9 (2003)
3. W.-R. Hu and Y.-L. Wu, *Natl. Sci. Rev.* **4**, 5 (2017).
4. Z. Luo, Y. Wang, Y. Wu, W. Hu and G. Jin, *Prog. Theor. Exp. Phys.* (2020).
5. Z. Luo, Z. Guo, G. Jin, Y.-L. Wu and W. Hu, *Results Phys.* **16**, 102918 (2019).
6. W. Ruan, C. Liu, Z. Guo, Y. Wu and R. Cai, *Nat. Astron.* **4**, 108–109 (2020).
7. Xinhua (2019, September 20). China Focus: Chinese satellite tests space-based gravitational wave detection technologies. *XINHUANET*. Retrieved from http://www.xinhuanet.com/english/2019-09/20/c_138408486.htm
8. Z. Luo, H. Liu and G. Jin, *Opt. Laser Technol.* **105**, 146–151 (2018).
9. J. Deng, Z.Cai, K. Chen, X. Shi, J. Yu and H. Li. *Chin. Opt. Lett.* **12**, 503–514 (2019).
10. Y. Wang, K.-Q. Qi, S. Wang, W. Li, Z. Li and Z. Wang, *IEEE Access* PP (2019), 1–1.
11. J. He, P. Liu, R. Gao, C. Xue, L. Ma, L. Duan and Q. Kang, *Plasma Sci. Technol.* **22**, 094002 (2020)
12. J. He, L. Ma, S. Xue, C. Zhang, L. Duan and Q. Kang, *Plasma Sci. Technol.* **20**, 025403 (2018).
13. G. Potrivitu, Y. Sun, M. W. A. Rohaizat, O. Cherkun, L. Xu, S. Huang and S. Xu, *Aerospace* **7**, 67 (2020).
14. G. Potrivitu, L. Xu, S. Huang, M. W. A. Rohaizat and S. Xu, *J. Appl. Phys.* **127**, 064501 (2020).

15. L. J. W. Mark, I. Levchenko, M. W. A. Rohaizat, S. Huang, L. Xu, Y. Sun, G. Potrivitu, J. Yee, R. Sim, Y. Wang, S. Levchenko, K. Bazaka and S. Xu, *J. Vis. Exp.* **144**, e58466 (2019).
16. G. Anderson, J. Anderson, M. Anderson, G. Aveni, D. Bame, P. Barela, K. Blackman, A. Carmain, L. Chen, M. Cherng, S. Clark, M. Connally, W. Connolly, D. Conroy, M. Cooper, C. Cutler, J. D'Agostino, N. Demmons and E. Dorantes, *Phys. Rev. D* **98**, 102005 (2018).
17. J. Boeuf, *J. Appl. Phys.* **121**, 011101 (2017).
18. F. Acernese, F. Barone, R. De Rosa, A. Eleuteri, S. Pardi, L. Milano and G. Russo, *Class. Quantum Grav.* **21**, S1849 (2004).
19. B. Allen, W. Anderson, P. Brady, D. Brown and J. Creighton, *Phys. Rev. D* **85**, 2–4 (2005).
20. H. Rakshit, *Int. J. Eng. Technol.* **7**, 1151–1162 (2015).